Equilibrium Cross Sectional Area at Tidal Inlets

Steven A. Hughes[1]

[1]US Army Engineer Research and Development Center
Coastal and Hydraulics Laboratory
3909 Halls Ferry Road
Vicksburg, MS 39180-6199, USA
Steven.A.Hughes@erdc.usace.army.mil

ABSTRACT

HUGHES, S.A., 2002. Equilibrium cross sectional area at tidal inlets. *Journal of Coastal Research*, 18(1), 160–174. West Palm Beach (Florida), ISSN 0749-0208.

A relationship is derived between the tidal prism passing through an inlet and the inlet throat minimum cross-sectional area. The form of the new relationship closely resembles previous empirical formulations. The main assumption in the derivation is that the maximum discharge per unit width through an inlet is at equilibrium with every depth across the minimum cross section. The derived relationship matches data from 102 U.S. inlets as well as results from 18 small-scale movable-bed models, whereas previous empirical relationships failed to match the laboratory data.

The new relationship between tidal prism and equilibrium cross-sectional area is used to derive new scaling relationships for movable-bed tidal inlet laboratory models. The scaling assures that the relative balance between the turbulent shear stress acting on the bottom and the critical shear stress of the bed material is the same in the model as in prototype. These scaling relationships will allow quantitative results of complicated inlet processes to be obtained from properly operated small-scale movable-bed inlet models.

ADDITIONAL INDEX WORDS: *Tidal inlets, tidal prism, equilibrium area, movable-bed models, scale relationships, inlet equilibrium.*

INTRODUCTION

It has been long recognized that a relationship exists between the minimum cross-sectional area of a stable tidal inlet and the tidal prism flowing through the inlet during half of the tidal cycle. This relationship has been most often expressed as a dimensionally nonhomogeous equation of the form

$$A_c = CP^k \qquad (1)$$

where A_c is the minimum equilibrium cross-sectional area, and P is the tidal prism (the amount of water that flows into the inlet during flood tide or out of the inlet during the ebb tide). Values for the coefficient and exponent (C, k) are determined empirically by plotting values of inlet area versus tidal prism for actual inlets. The dimensionless exponent k has values ranging between 0.84 and 1.10 (JARRETT, 1976) with the scaling coefficient C acquiring the dimensions necessary for dimensional balance in view of the selected exponent.

O'BRIEN (1976) showed that a regime equation (LACEY, 1929) for equilibrium flow in nonsilting, nonscouring irrigation channels could be expressed in the form of Eqn. 1 with $k = 0.83$ by substituting equations for critical velocity and maximum discharge expressed in terms of the tidal prism and cross-sectional area. MASON (1973) performed a similar comparison with two other regime equations, and he found that O'BRIEN's (1931) formula relating A_c and P agreed quite

well with the regime equation of SIMONS and ALBERTSON (1963) with $k = 0.86$ provided average discharge was used rather than maximum discharge.

JARRETT (1976) summarized earlier empirical expressions of the form given by Eqn. 1 for the A_c versus P relationship (hereafter referred to as the "*tidal prism relationship*") given by LeCONTE (1905), O'BRIEN (1931, 1969), NAYAK (1971), and JOHNSON (1972). Jarrett then improved the tidal prism relationship by gathering and examining data for 108 tidal inlets on the Atlantic, Gulf, and Pacific Coasts of the United States.

The inlets in Jarrett's study were divided into three main categories according to whether they had no jetties, one jetty, or two jetties. Within each category the inlets were further separated into groups corresponding to the three coasts. Regression analyses were performed to determine the best fit of Eqn. 1 to data within the various groupings, and the resulting empirical equations were presented in U.S. customary units with A_c having units of ft^2 and P having units of ft^3. Jarrett's results are still the best available predictors for inlet equilibrium cross-sectional area.

KRISHNAMURTHY (1977) derived a theoretical expression for the tidal prism versus equilibrium cross-sectional area relationship by assuming a logarithmic profile over the water depth and integrating the profile across a rectangular cross section. At equilibrium, maximum bottom shear stresses were represented by the critical shear stress. The resulting simplified expression in the form of Eqn. 1 had an exponent of $k = 1.0$ and a coefficient C that was inversely proportional

to tidal period, friction velocity, and a term that included tidal amplitude, mean channel depth, and roughness coefficient. Krishnamurthy analyzed the importance of each parameter and concluded that grain size of the bed material and roughness of the channel had minor influence for prototype-scale tidal inlets. Also, the tidal range had little influence provided the mean channel depth is sufficiently deep. Comparison to 26 West Coast tidal entrances was good, and this lent theoretical justification to O'BRIEN's (1931) empirical tidal prism versus equilibrium area relationship.

Stable inlets, where the minimum cross-sectional area remains relatively constant, represent a dynamic balance between the tidal flow and the littoral sediments. Sediment moving along the coast is deposited into the inlet, and the tidal (and riverine) flow moves the sediment out of the inlet throat. Some littoral sediment is deposited on the flood shoal, some is deposited on the ebb shoal, and some sediment moves along the ebb shoal and adjacent attachment bar to continue down drift.

As summarized by KRAUS (1998), several researchers have noted that reduced littoral transport results in a larger equilibrium cross-sectional area A_c for the same tidal prism P because less material has to be removed from the inlet throat during each tidal cycle. Consequently, inlets situated on coasts with reduced littoral drift tend to follow a tidal prism relationship (Eqn. 1) that has a larger value of the empirical coefficient C and a decreased value of the empirical exponent k.

For unjettied and single-jetty inlets JARRETT (1976) found that values of A_c for Pacific Coast inlets were smaller than inlets on the Atlantic and Gulf Coasts having the same values of P. He attributed the difference to greater littoral material being deposited in the Pacific Coast inlets leaving relatively less tidal energy for expanding the inlet area. BRUUN (1978, p. 318) disputed the part of this explanation pertaining to decreased tidal energy for inlet expansion, and instead suggested the difference perhaps stemmed from the Pacific Coast inlets having more "flow-efficient" cross sections typified by smaller area but deeper depths. This argument is supported by the fact that the average ratio of width to hydraulic radius (W/R) was smaller for the Pacific Coast inlets, but no adequate explanation was given for why Pacific Coast inlets should have smaller values of W/R. Bruun also noted that dual-jettied inlets tend to have smaller equilibrium cross sections for two reasons: (1) the jetties "organize" the flow so it is more efficient for removing sediment, and (2) the jetties help decrease the amount of littoral material that enters the inlet throat.

BRUUN (1978) summarized his earlier work proposing the ratio of tidal prism to gross longshore sediment transport rate (P/Q_g) as a criterion for relative stability of inlet throat cross-sectional area for relatively small channels. Values of $P/Q_g > 150$ imply the tidal prism is sufficient to sweep the inlet throat clean of littoral sediments, but decreasing stability occurs as the ratio P/Q_g becomes smaller than 100.

KRAUS (1998) introduced a rather elegant derivation of a process-based model that balances the transporting capability of the tidal and riverine flow with the longshore sediment transport tending to infill the channel. At equilibrium the

model recovered an analytical form of the tidal prism relationship given by the expression

$$A_e = \left[\frac{\alpha \pi^3 C_k^3 n^2 W^{4/3}}{Q_g T^3} \right]^{0.3} P^{0.9} \qquad (2)$$

where

α—empirical coefficient ≈ 1.0
C_k—non-sinusoidal tide factor ($0.81 \leq C_k \leq 1.0$)
n—Manning coefficient in units of s/m$^{1/3}$
W—equilibrium channel width
Q_g—gross longshore sediment transport rate
T—tidal period

Kraus's derivation gives an analytical expression for the C coefficient in Eqn. 1. Equation 2 is dimensionally consistent, but care must be taken when evaluating the equation in units other than SI because Manning's coefficient is normally specified in metric units. The equilibrium cross-sectional area is strongly dependent on tidal prism and tidal period, with weaker dependence on channel width and gross longshore transport rate. Kraus noted that the inverse dependence on Q_g is consistent with the observation that equilibrium cross-section area is smaller in regions with higher littoral transport.

Application of Eqn. 2 to limited data given by BRUUN (1978) demonstrated correct trends and reasonably good agreement. However, because the development is based on a balance between tidal flow rate and alongshore sediment transport rate, applying Eqn. 2 at sheltered locations having little or no longshore transport may become problematic because the inverse dependence on Q_g could make the cross-sectional area unrealistically large. Nevertheless, Eqn. 2 should provide good equilibrium area estimates even when using approximate estimates of the gross longshore transport rate.

The empirical formulas presented by JARRETT (1976) provide reasonable fits to available data for most typical inlets around the U.S. coastline. However, results from much smaller inlets do not match the empirical formulations, and instead exhibit equilibrium cross-sectional areas that are much larger than predicted by the tidal prism relationships.

BYRNE et al. (1980) studied fourteen inlets in the lower Chesapeake Bay in terms of the A_e versus P relationship. They noted a departure from established tidal prism relationships for inlets having $A_e < 100$ m^2. They also noted reduced values of W/R and decreased values of mean maximum velocity for smaller inlets when compared to oceanic inlets. Small-scale movable-bed model studies of tidal inlets presented by MAYOR-MORA (1977) and SEABERGH et al. (2001) continued this same trend with even greater departure from the predictions given by Jarrett's empirical relationships.

Figure 1 presents 90 values of A_e versus P for full-sized inlets given by JARRETT (1976), 12 Chesapeake Bay inlets described by BYRNE et al. (1980), 11 small-scale model inlets given MAYOR-MORA (1977), and 7 small-scale model inlets from SEABERGH et al. (2001). Nineteen of the inlets tabulated by Jarrett did not include values for the equilibrium width (used later) so they were not included on the plot. The solid
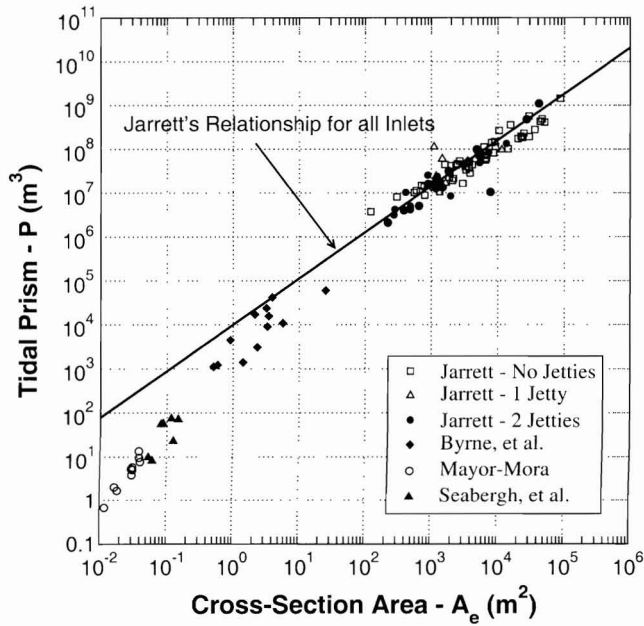
Figure 1. Equilibrium cross-section area versus tidal prism for field and laboratory data.

Definition Sketch

Figure 2. Idealized velocity distribution for fully developed flow.

line on Figure 1 is the JARRETT's (1976) empirical expression for all inlets, given in SI units as

$$A_e = 1.576(10)^{-4}P^{0.95} \qquad (3)$$

The cross-sectional areas measured at equilibrium in the small-scale laboratory data and some of the Chesapeake Bay data are an order of magnitude larger than would be predicted by Eqn. 3. This indicates the relationship between tidal prism and equilibrium cross-section area relies on additional physical parameters as indicated by Kraus's derived result shown in Eqn. 2. These additional parameters might not vary significantly over the range of coastal inlets studied by Jarrett, but they probably have an impact at the greatly reduced size of the laboratory data.

The following sections of this paper present a derivation of the A_e versus P tidal prism relationship based on the concept of equilibrium depth associated with maximum discharge per unit width. This is quite similar to the approach followed by KRISHNAMURTHY (1977). The derived expression appears to be valid for all data, including small-scale laboratory inlets, and it provides an explanation for observed reduction in mean maximum velocity at smaller inlets. Finally, because the new area-prism relationship spans inlets of all sizes, a proposed scaling law is derived that facilitates movable-bed modeling of inlet channels in small-scale laboratory model basins.

MAXIMUM EQUILIBRIUM DISCHARGE PER UNIT WIDTH

The concept of maximum equilibrium discharge per unit width assumes that a given channel depth under a condition of live-bed sediment transport can tolerate up to a critical value of water discharge per unit channel width without additional erosion of the bed. The critical value of discharge is termed the *"maximum equilibrium discharge"* and the corresponding channel depth is the *"equilibrium scour depth"*.

Formulation

Assume the vertical velocity profile during maximum discharge through a tidal inlet can be represented as a steady, fully-developed, rough turbulent boundary layer extending from the bottom to the free surface as sketched in Figure 2. Any contribution by waves to this quasi-steady flow situation is neglected. The boundary layer velocity profile can be adequately approximated by a 1/8-power curve (YALIN, 1971) with vertical velocity variation with depth from the water surface ($h = 0$) approximated as

$$V(h) = \frac{9V_m}{8}\left(1 - \frac{h}{h_e}\right)^{1/8} \qquad (4)$$

and the shear stress at the bed given by

$$\tau_o = \rho_w \left[\frac{V_m}{C_\tau (h_e/d_e)^{1/8}} \right]^2 \qquad (5)$$

where

ρ_w—mass density of water

V_m—depth-averaged velocity

C_τ—undetermined constant

h_e—equilibrium water depth at maximum discharge

d_e—median grain-size diameter

The constant C_τ is a boundary layer shape factor that includes the unknown relationship between d_e and bottom roughness.

The *Critical Shear Stress* of the *noncohesive* sand bed is given by the Shields parameter as

$$\tau_{cr} = C_s (\rho_s - \rho_w) g d_e \qquad (6)$$

with

C_s—constant of proportionality

ρ_s—mass density of sand

g—gravitational acceleration

d_e—median grain-size diameter

For live-bed equilibrium, a shear stress balance is assumed with $\tau_o \sim \tau_{cr}$. Equating Eqns. 5 and 6 results in the expression

$$\frac{h_e}{d_e} = \frac{1}{(C_e)^8} \left[\left(\frac{\rho_w}{\rho_s - \rho_w} \right) \left(\frac{V_m^2}{g d_e} \right) \right]^4 \qquad (7)$$

where the two unknown constants, C_τ and C_s, have been combined into the shear stress proportionality constant C_e. The term in square brackets on the right-hand side of Eqn. 7 is the ratio of grain-size Froude number to the immersed specific gravity of the sand, and it is defined as the *Grain Mobility Number* (YALIN, 1971).

A more useful form of Eqn. 7 is obtained by multiplying both sides by h_e^8 and rearranging to get an expression for the equilibrium discharge per unit width, i.e.,

$$q_e = C_e |g(S_s - 1)|^{1/2} d_e^{3/8} h_e^{9/8} \qquad (8)$$

where the q_e is defined as the **Equilibrium Maximum Discharge per unit width**, given by

$$q_e = V_m h_e \qquad (9)$$

and $S_s = \rho_s/\rho_w$ is the sediment specific gravity (about 2.65 for quartz sand). As expected Eqn. 8 indicates that the equilibrium maximum discharge is primarily a function of water depth with sediment size having a relatively minor effect.

Empirical Coefficient

The unknown coefficient in Eqn. 8 was empirically evaluated by comparison to field measurements at two dual-jetty tidal inlets. Vertical profiles of horizontal velocity were measured along transects at Shinnecock Inlet, New York, and at Ponce de Leon Inlet, Florida, using a boat-mounted acoustic Doppler current profiler. Discharge per unit width was estimated from the measurements by integrating the velocity profiles over the depth. Profiling transects across the inlet throats occurred at or around the maximum ebb or flood flow.
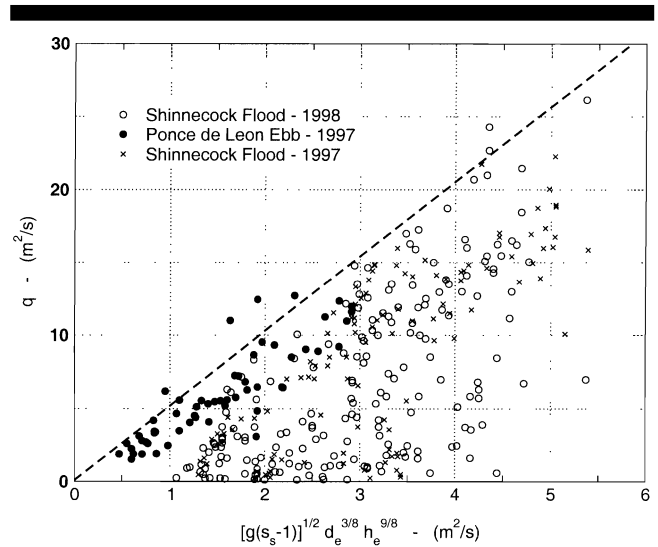
Figure 3. Field data from two dual-jettied inlets.

The results are shown on Figure 3 where calculated discharge per unit width is plotted versus the term $[g(S_s - 1)]^{1/2} d_e^{3/8} h_e^{9/8}$ on the right-hand side of Eqn. 8. Grain-size for the Shinnecock Inlet channel was taken as 0.6 mm, whereas a size of 0.21 mm was used for Ponce de Leon Inlet. Both sands were assumed to have the same density as quartz.

The data points on Figure 3 show a wide range of discharge per unit width measured at the different depths. However, there is an upper limit to the data as indicated by the straight dashed line. This dashed line represents the maximum discharge per unit width (q_e) that can be sustained at a particular value of the parameter $[g(S_s - 1)]^{1/2} d_e^{3/8} h_e^{9/8}$. The discharge indicated by the dashed line is termed the **equilibrium maximum discharge**. Any increase in discharge beyond the equilibrium value will result in an increase in water depth at that location.

The scatter of measurements beneath the dashed line is pronounced, and this indicates that the discharge calculated for those measurements was less than could be tolerated by the depth at that location. Points just beneath the dashed line might be locations where the present bottom was eroded by discharges slightly greater than those measured during the field exercises, and hence the measured discharge was not the maximum equilibrium discharge. Many of the data points well below the line came from inlet cross-sections either slightly seaward of the jetties where depths are determined by waves and longshore currents in addition to tidal discharge; or landward of the entrance channel where the tidal current is insufficient to scour the channel, and depths have been increased by interior channel dredging.

Another explanation for data scatter below the dashed line is that depths at some of the locations are scoured by a different cross-channel flow distribution that occurs during the reverse maximum tidal flow. HUGHES (2000) showed that the cross-channel flow distribution during flood tide at Shinnecock Inlet is controlled by the offset jetty configuration that

forces the flow to favor one side of the channel. During ebb tide, a different cross-channel flow distribution dominates.

Finally, there is the possibility that some of the depths are the result of scouring that occurred during episodic events such as storm surges or river discharge combined with ebb flow, or the depths are remnants of shifting channels that are now undergoing shoaling. Regardless of the reason, depths associated with data points below the dashed line (in theory) are not in equilibrium with the measured discharge. In other words these depths would be able to accommodate increased flow discharge without additional scouring of the bottom.

The dashed line in Figure 3 corresponds to $C_e = 5.12$ in Eqn. 8, which can now be expressed as an empirical equation for equilibrium maximum discharge per unit width, i.e.,

$$q_e = 5.12[g(S_s - 1)]^{1/2}d_e^{3/8}h_e^{9/8} \tag{10}$$

The **equilibrium scour depth**, h_e, associated with the equilibrium discharge q_e and noncohesive sediment is obtained by rearranging Eqn. 10 into the form

$$h_e = \frac{0.234q_e^{8/9}}{[g(S_s - 1)]^{4/9}d_e^{1/3}} \tag{11}$$

where the depth h_e, is taken relative to the tide level at maximum discharge. Although it might be possible to have depths greater than the equilibrium scour depth, these depths would have to be caused by some process other than the maximum discharge at that location. Estimates of equilibrium scour depth from Eqn. 11 should be considered conservative because the estimates represent the outer envelope of the field data. In reality the maximum discharge per unit width may not persist long enough to allow scoured depths to reach the predicted equilibrium depth, particularly in regions where significant quantities of littoral sediment are deposited during each tide cycle.

Finally, substitution of the value of C_e into Eqn. 7 and rearranging provides a relationship for mean velocity at a location in terms of the equilibrium depth and sand parameters, i.e.,

$$V_m = 5.12[g(S_s - 1)]^{1/2}d_e^{3/8}h_e^{1/8} \tag{12}$$

An equation similar to Eqn. 11 was proposed by THOMAS and PRASUHN (1977) for equilibrium depth in natural rivers. (Their original derivation used customary U.S. units, but the result is presented here in SI units.) They began with the Manning equation

$$Q_m = \frac{A_eR^{2/3}S^{1/2}}{n} \tag{13}$$

where Q_m is total discharge, A_e is cross-sectional area, R is hydraulic radius, S is channel slope, and n is Manning's coefficient. Then S was replaced from Einstein's flow intensity equation with $\Psi = 30$ for zero transport; n was replaced with the Strickler equation; it was assumed $R \approx h_e$; and for a rectangular cross-section $A_e = h_eW$ and $Q_m = q_eW$. This yielded the dimensionally nonhomogeneous expression (here in SI units) with a coefficient having dimensions of $(m^{1/2}/s)$.

$$h_e = \left[\frac{q_e}{4.4(S_s - 1)^{1/2}d_e^{1/3}}\right]^{6/7} \quad \text{THOMAS and PRASUHN (1977)} \tag{14}$$

Recognizing the units of the coefficient are the same as the square root of gravity, Eqn. 11 can be made dimensionally homogeneous by including the gravitational constant to give

$$h_e = \frac{0.75q_e^{6/7}}{[g(S_s - 1)]^{3/7}d_e^{2/7}} \tag{15}$$

The resulting expression is very similar to Eqn. 11, and it can be used with any consistent set of units.

Application of the Equilibrium Discharge Relationship

To test the validity of the equilibrium maximum discharge relationship given by Eqn. 10, the relationship was used to estimate the total maximum discharge at Matagorda Entrance Channel located in Texas on the Gulf of Mexico. The entrance channel, shown in Figure 4, features parallel jetties spaced about 610 m apart on the Gulf of Mexico side. The jetties than have a transition to a narrower channel with a separation distance of about 317 m at the transition and a slightly less separation of about 284 m at the bay-side termination of the jetties. During flood tide the jetty system funnels the tidal flow which has resulted in severe scour throughout the narrow portion of the inlet.

Cross-section profiles recorded in the narrow section are shown in Figure 5. The profiles are plotted in original U.S. customary units of *feet* with the left side of the plot being the west side of the entrance channel. In other words, the view of the profile is from the Gulf of Mexico looking toward Matagorda Bay. Station +00+00 is located at the landward end of the narrowing transition section, Station +02+00 is at the midway point of the narrow section, Station +03+00 is located at the end shorter (east) jetty, and Station +03+70 is at the end of the west jetty.

Under the assumption that all profiles represent the equilibrium maximum depths with quartz sand ($S_s = 2.65$) having a median grain-size of 0.18 mm (0.00018 m), Eqn. 10 was applied at every measured depth along each of the profiles shown on Figure 5. This resulted in an estimated cross-channel distribution of maximum discharge. Integrating the discharge distributions over the entire profile provided an estimate of total maximum discharge at each profile location. These estimates are tabulated in Table 1.

Measured total maximum discharge at Matagorda Entrance Channel on ebb tide (which is assumed to be similar to flood tide values) is 7,360 m³/s. Although the estimates of maximum total discharge based solely on depth profiles and sediment grain-size have about 18 percent variation between highest and lowest, the estimates bracket the measured peak total quite well.

The application to Matagorda Entrance Channel provides additional confirmation that the empirical equation for maximum equilibrium discharge per unit width (Eqn. 10) gives reasonable estimates. Furthermore, it provides encouragement that relating cross-sectional area to maximum total discharge by integrating Eqn. 10 across the channel is a viable

Figure 4.   Aerial view of Matagorda Entrance Channel, Texas.

approach for developing an A_e versus P tidal prism relationship. This integration is performed in the following section.

CROSS-SECTION AREA VERSUS TIDAL PRISM RELATIONSHIP

In this section a relationship is derived relating the minimum inlet throat cross-sectional area at mean sea level to the tidal prism flowing through the inlet during spring tide. The derived relationship takes a form similar to the empirical relationships given by O'BRIEN (1931, 1969) and JARRETT (1976) for tidal inlets assumed to be at, or near, an equilibrium condition.

The main assumption in this derivation is that the minimum inlet cross-sectional area needed to accommodate a given maximum total discharge will occur when the equilibrium discharge condition given by Eqn. 10 is fulfilled at every depth along the cross section. As mentioned earlier, at most inlets during either flood or ebb tide there are likely to be portions of the cross section that experience less flow than

could be accommodated by the depth because of different flow patterns during flood or ebb, or channel maintenance dredging, or migration of the primary flow channels. Consequently, the A_e versus P expression developed below estimates the minimum possible cross-sectional area.

Derivation of A_e versus Q_m Relationship

During the maximum spring tide, it is assumed the discharge at every location along the minimum cross section profile is given by Eqn. 10, the total maximum discharge, Q_m, is found by integrating the maximum discharge per unit width over the equilibrium width, W, of the inlet, or

$$Q_m = \int_0^W dQ = \int_0^W q_e \, dy \qquad (16)$$

Representing Eqn. 10 as

$$q_e = f_s h_e^{9/8} \qquad (17)$$

where
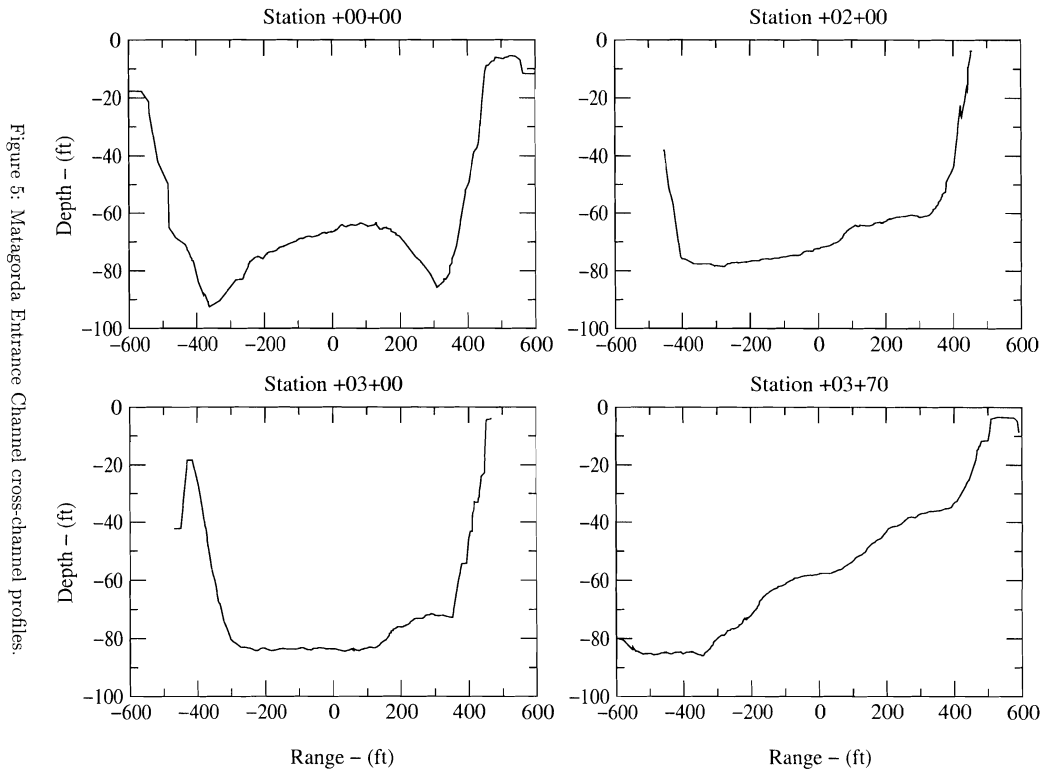
Figure 5. Matagorda Entrance Channel cross-channel profiles.

$$f_s = 5.12[g(S_s - 1)]^{1/2} d_e^{3/8} \qquad (18)$$

the maximum discharge becomes

$$Q_m = f_s \int_0^w h_e^{9/8} \, dy \qquad (19)$$

The equilibrium cross-sectional area, A_e, is simply

$$A_e = \int_0^w h_e(y) \, dy \qquad (20)$$

where $h_e(y)$ is the equilibrium depth variation along the cross section.

Trapezoidal Cross Section

For the trapezoidal cross section illustrated in Figure 6, the cross-sectional area is given by

Table 1. *Estimated maximum discharge at Matagorda Entrance Channel.*

Cross-Section Label	Max. Discharge (m³/s)
+00+00	7,860
+02+00	6,610
+03+00	7,140
+03+07	7,130
Average	7,185

$$A_e = h_o \left(\frac{y_1 + y_3}{2} + y2 \right) \qquad (21)$$

and the total maximum discharge from Eqn. 19 is

$$Q_m = f_s \int_0^{y_1} \left(\frac{h_o y}{y_1} \right)^{9/8} dy + f_s \int_0^{y_2} (h_o)^{9/8} \, dy \qquad (22)$$

$$+ f_s \int_0^{y_3} \left(\frac{h_o y}{y_3} \right)^{9/8} dy \quad \text{or}$$

$$Q_m = f_s h_o^{9/8} \left[\frac{8}{17}(y_1 + y_3) + y_2 \right] \qquad (23)$$

Solving Eqn. 21 for h_o and substituting into Eqn. 23, and
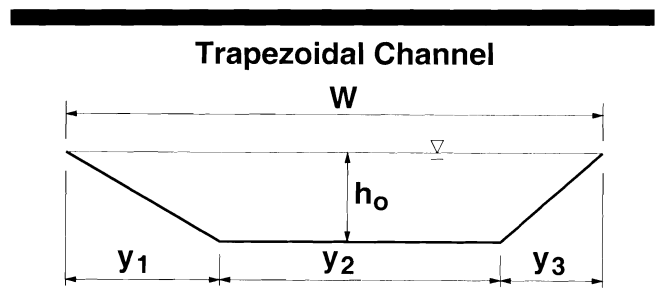
Figure 6. Trapezoidal cross section definition sketch.

Parabolic Channel
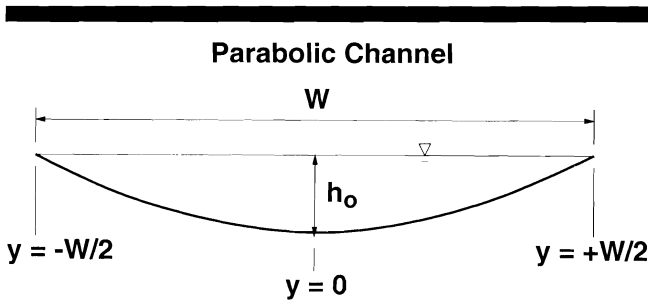
Figure 7. Parabolic cross section definition sketch.

rearranging yields the following expression for equilibrium minimum area versus maximum total discharge

$$A_c = \left[\frac{\frac{1}{2}(y_1 + y_3) + y_2}{\left[\frac{8}{17}(y_1 + y_3) + y_2\right]^{8/9}} \right] \frac{1}{f_s^{8/9}} Q_m^{8/9} \qquad (24)$$

The limits of the coefficient in the large square brackets can be examined by considering the two limiting special cases. First, when $y_1 = y_3 = 0$, the channel is a constant-depth rectangle with width $W = y_2$. In this case Eqn. 24 becomes

$$A_c = 1.0 \frac{W^{1/9}}{f_s^{8/9}} Q_m^{8/9} \qquad (25)$$

Second, when $y_2 = 0$, the channel is triangular with width $W = (y_1 + y_3)$, and Eqn. 24 reduces to

$$A_c = 0.977 \frac{W^{1/9}}{f_s^{8/9}} Q_m^{8/9} \qquad (26)$$

Parabolic Cross Section

A nearly identical result stems from assuming the inlet cross section to be a parabolic shape as illustrated in Figure 7 with the depth given by the expression

$$h_c(y) = h_o \left[1 - 4\left(\frac{y}{W}\right)^2 \right] \qquad (27)$$

For this case the cross-sectional area is given by

$$A_c = \int_{W/2}^{+W/2} h_c(y)\, dy = \int_{W/2}^{+W/2} h_o \left[1 - 4\left(\frac{y}{W}\right)^2 \right] dy$$

$$= \frac{2}{3} h_o W \qquad (28)$$

and the maximum discharge is found as

$$Q_m = f_s \int_{W/2}^{+W/2} |h_c(y)|^{9/8}\, dy$$

$$= f_s h_o^{9/8} \int_{W/2}^{+W/2} \left[1 - 4\left(\frac{y}{W}\right)^2 \right]^{9/8} dy \qquad (29)$$

Recognizing the integrand is symmetric, and rearranging gives

$$Q_m = f_s h_o^{9/8} 2 \left(\frac{4}{W^2}\right)^{9/8} \int_0^{W/2} \left[\left(\frac{W}{2}\right)^2 - y^2 \right]^{9/8} dy \qquad (30)$$

The integral is now in the form of a definite integral given in standard math tables as

$$\int_0^{W/2} \left[\left(\frac{W}{2}\right)^2 - y^2 \right]^{9/8} dy = \left[\frac{\Gamma\left(\frac{1}{2}\right)\Gamma\left(\frac{17}{8}\right)}{2\Gamma\left(\frac{21}{8}\right)} \right] \left(\frac{W}{2}\right)^{13/4} \qquad (31)$$

which yields a maximum discharge for the parabolic channel of

$$Q_m = \left[\frac{\Gamma\left(\frac{1}{2}\right)\Gamma\left(\frac{17}{8}\right)}{2\Gamma\left(\frac{21}{8}\right)} \right] f_s h_o^{9/8} W \qquad (32)$$

Solving Eqn. 28 for h_o and substituting into Eqn. 32, and then rearranging yields the following expression for A_c versus Q_m

$$A_c = \frac{2}{3} \left[\frac{2\Gamma\left(\frac{21}{8}\right)}{\Gamma\left(\frac{1}{2}\right)\Gamma\left(\frac{17}{8}\right)} \right]^{8/9} \frac{W^{1/9}}{f_s^{8/9}} Q_m^{8/9} \qquad (33)$$

The numerical coefficient in Eqn. 33 evaluates to 0.985, while the rest of the equation is identical to Eqns. 25 and 26 found for the trapezoidal channel.

Because any arbitrary inlet cross section can be represented as a discrete series of narrow trapezoids, it should be expected that the general A_c versus Q_m relationship will also yield a numerical coefficient very close to unity. Given the small variation seen in the numerical coefficients between Eqns. 25, 26, and 27 (0.977 to 1.0), it is reasonable to set the numerical coefficient equal to unity.

However, as noted earlier, this derivation assumes that at each point across the entire cross section the discharge is the maximum it can reach without causing additional erosion. Evidence from numerous inlets indicates this is not the case, and the inlet minimum cross section could, in fact, accommodate additional discharge. Therefore, an empirical factor, k_a, is included that will have a value greater than unity; and the final proposed A_c versus Q_m relationship is given as

$$A_c = k_a \frac{W^{1/9}}{f_s^{8/9}} Q_m^{8/9} \qquad (34)$$

where an appropriate value of k_a will be established using measured field and laboratory data.

Derivation of A_c versus P Relationship

Following the lead of previous investigators (e.g., KEULEGAN and HALL, 1950, KRAUS, 1998), the tide is assumed to be sinusoidal with the time-dependent total discharge, Q, given by

$$Q(t) = S_b \frac{d\eta}{dt} = S_b a_t \left(\frac{2\pi}{T}\right) \cos\left(\frac{2\pi t}{T}\right) \qquad (35)$$

where

S_b—bay surface area (assume vertical side walls)

η—time-dependent tide elevation $[=a_t \sin(2\pi t/T)]$

a_t—tidal amplitude

T—tidal period

t—time

Noting that the *"tidal prism"* is defined as $P = 2a_t S_b$, the maximum total discharge, Q_m, is written simply as

$$Q_m = \frac{\pi P}{T} \qquad (36)$$

KEULEGAN and HALL (1950) included a coefficient C_k ranging between 0.81 to 1.0 to account for more realistic non-sinusoidal tides, but for this derivation it is assumed that the effects of non-sinusoidal tides will be included in the empirical factor, k_a.

Substituting Eqn. 36 for Q_m and Eqn. 18 for f_s in Eqn. 34 results in the tidal prism relationship

$$A_e = 0.65 k_a \left[\frac{W^{1/9}}{[g(S_s - 1)]^{4/9} d_e^{1/3} T^{8/9}}\right] P^{8/9} \qquad (37)$$

Equation 37 has the familiar form of the tidal prism relationship (Eqn. 1), and it bears a close similarity with the processes-based derivation expression (Eqn. 2) derived by KRAUS (1998) with the main difference being Kraus's inclusion of the alongshore sediment transport rate. The coefficient in square brackets in Eqn. 37 is strongly dependent on tidal period (T), weakly dependent on median grain size (d_e), and only slightly dependent on channel width (W).

Comparison to Field and Laboratory Data

To facilitate comparison with data, Eqn. 37 was rearranged into the form

$$A_e = 0.65 k_a (C_I P)^{8/9} \qquad (38)$$

where

$$C_I = \left[\frac{W^{1/8}}{[g(S_s - 1)]^{1/2} d_e^{3/8} T}\right] \qquad (39)$$

All of the field and laboratory data represented on Figure 1 have been replotted on Figure 8 with values of A_e on the abscissa and corresponding values of $C_I P$ (termed *"modified tidal prism"*) on the ordinate. Sediment sizes for the laboratory data were 0.34 mm for the MAYOR-MORA (1977) data, and 0.13 mm and 0.26 mm for the SEABERGH *et al.* (2001) data. Representative grain-sizes for 43 of the 90 inlets from JARRETT'S (1976) report were provided by CARR (1999) and by STAUBLE (*personal communication*). A grain size of 0.25 mm was assumed for the remaining inlets including the Chesapeake Bay data. This assumption was deemed reasonable because of the relatively minor influence grain size ($d_e^{1/3}$) is expected to have over the range of typical sediments sizes found at tidal inlets.

The lighter dashed line is Eqn. 38 plotted using a value of
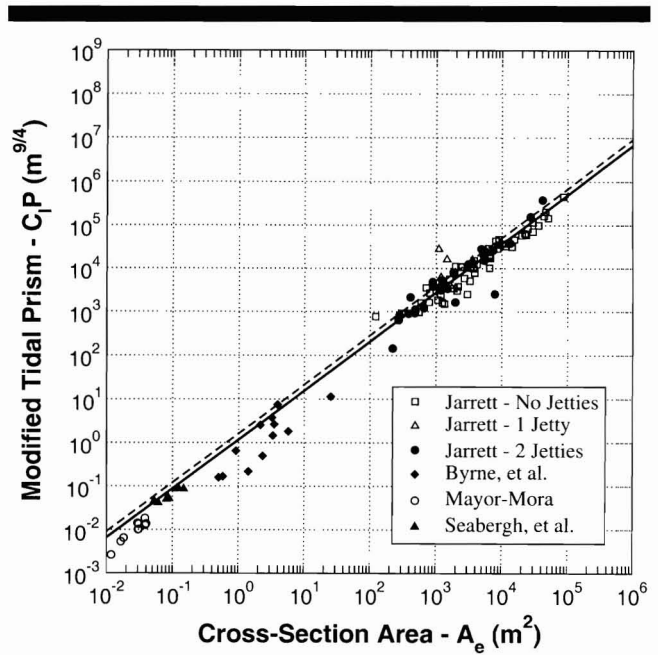
Figure 8. Field and laboratory data compared to new tidal-prism relationship.

$k_a = 1$, representing the minimum cross-section area with maximum non-scouring discharge at every point. As seen, most of the data have greater values of A_e and lie to the right of the dashed line.

The heavier solid line on Figure 8 is a best-fit regression for the coefficient k_a using all the data equally weighted. The regression gave a value of $k_a = 1.34$ with a correlation coefficient of 0.93 and a root-mean-square error of 1.5 percent. Because of the relatively few number of laboratory points (18), the best-fit analysis is weighted toward the 90 full-scale inlets.

The best-fit value of k_a implies that, on average, tidal inlets near equilibrium have minimum cross-sectional areas that are 34% larger than the minimum predicted under the assumption of an equilibrium scour depth associated with a maximum discharge per unit width. However, recall that the non-sinusoidal C_k factor was included in k_a, so within the range $0.81 \le C_k \le 1.0$ the variation would be 11–34%. This variation in A_e could be related to a number of factors including alongshore sediment transport rate as noted by KRAUS (1998), flow channeling during flood and ebb tide, or even inaccuracies in the data as noted by JARRETT (1976).

The main point made by Figure 8 is that the small-scale laboratory data are now included in this new tidal-prism relationship, whereas previous empirical expressions did not explain the deviation shown by small-scale inlets. (Note that relatively little improvement was seen for the Chesapeake Bay data.) The primary reason that laboratory data conform to the new tidal prism relationship given by Eqn. 37 is the inclusion of tidal period in the formulation. At small scale the relatively shorter tidal period results in relatively larger cross-section area predictions which correspond to observed

model behavior. For example, model tidal periods in the range of 1200 to 3600 seconds used by MAYOR-MORA (1977) result in cross-sectional area predictions that vary between 10 to 25 times greater than estimates made using Jarrett's empirical expression for all inlets (Eqn. 3).

Also note that using the longer diurnal tide for Gulf Coast inlets in Eqn. 37 predicts a value for A_c that is about 46% smaller than for East Coast inlets having the same tidal prism, and that trend corresponds with Jarrett's observation. BRUUN (1978) speculated that unjettied Gulf inlet cross-sectional areas were smaller because of reduced littoral transport which allowed the inlet channels on the Gulf to be more flow efficient.

The direct, but very weak, dependence of equilibrium area on the cross-section width W has negligible influence over the range of widths for most tidal inlets. Even in small-scale model inlets, the width factor is far less important than tidal period. For example, the effect of width in a small-scale inlet having a width that is 1/1000th the size of a typical ocean inlet is to reduce the value of A_c by about one-half. But at the same time, the reduced model tidal period will act to increase A_c by over an order of magnitude.

The inverse dependence of A_c on tidal period and weaker dependence on channel width was also shown by KRAUS (1998), so it is expected his relationship (Eqn. 2) would also provide a good fit to all the data shown in Figure 8. However, the inverse dependence of A_c on Q_g in Kraus's formulation precludes application where the alongshore sediment transport rate is very small or nonexistent, such as in laboratory models.

Final Forms of the Relationships

Using the empirically established value of $k_a = 1.34$, the new expressions relating the equilibrium inlet cross-section area to maximum total discharge are given by the equations

$$A_c = 0.313 \left[\frac{W^{1/9}}{[g(S_s - 1)]^{4/9} d_c^{1/3}} \right] Q_m^{8/9} \qquad (40)$$

(or solving for Q_m)

$$Q_m = 3.69 \left[\frac{[g(S_s - 1)]^{1/2} d_c^{3/8}}{W^{1/8}} \right] A_c^{9/8} \qquad (41)$$

and the equilibrium area versus tidal-prism relationship is

$$A_c = 0.87 \left[\frac{W^{1/9}}{[g(S_s - 1)]^{4/9} d_c^{1/3} T^{8/9}} \right] P^{8/9} \qquad (42)$$

Important Note: The above equations are dimensional homogeneous which means they can be applied using any consistent set of units. In particular, sediment grain size needs to be expressed in the same length unit used for the other parameters (typically either *meters* or *feet*.)

Average Inlet Velocity at Maximum Flow

A fairly commonly used term is the *"mean maximum velocity"* which is defined as the average velocity through the inlet cross section during maximum spring tide discharge. The mean maximum velocity is calculated as the ratio of total
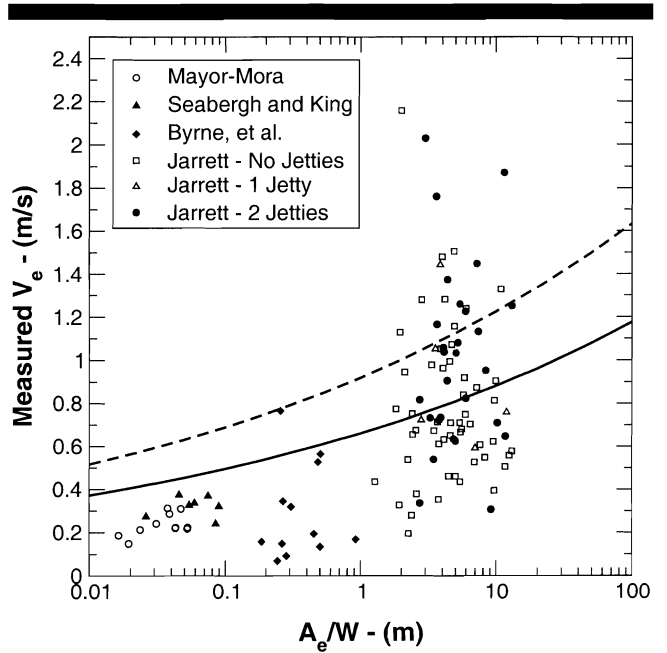
Figure 9. Mean maximum velocity as a function of inlet average depth.

maximum discharge to minimum cross-sectional area, i.e., $V_{MAX} = Q_m/A_c$, or substituting for Q_m from Eqn. 36.

$$V_{MAX} = \frac{\pi P}{T A_c} \qquad (43)$$

BRUUN (1978) noted that V_{MAX} tended to remain in the range between 0.9 to 1.2 m/s, and that a nominal value of $V_{MAX} = 1$ m/s is often used as a first approximation.

From Eqn. 41 V_{MAX} is estimated from the theory presented in this paper as

$$V_{MAX} = 3.69 [g(S_s - 1)]^{1/2} d_c^{3/8} \left(\frac{A_c}{W} \right)^{1/8} \qquad (44)$$

In theory the mean maximum velocity is nearly constant with only minor dependence on sediment properties, and a very weak dependence on the ratio A_c/W, which could be interpreted as *"average inlet depth."*

Figure 9 plots value of V_{MAX} estimated for the field and laboratory inlet data using Eqn. 43 versus A_c/W. The solid line is the theoretical expression of Eqn. 44 using a representative grain size of 0.25 mm. The dashed line represents the case where the entire cross section is carrying the maximum discharge per unit width ($k_a = 1.0$). The scatter seen in the data is profound, although there is an increasing trend in V_{MAX} as average inlet depth increases. The model-scale data all fall beneath the solid line, and that is a consequence stemming from the best-fit of the tidal prism relationship being influenced to a greater extent by the field data. Another possible explanation is that the laboratory velocities are small enough that bedforms could begin to influence the model results.

In general, inlets with no jetties tend to have more V_{MAX} values below the solid line than above, whereas inlets with

two jetties have the reverse trend. This corresponds with the observation that jettied inlets have more efficient flow channels and a reduction in minimum cross-section area. However, the wide scatter exhibited in Figure 9 indicates that the V_{MAX} parameter is probably not suitable as a general parameter for describing tidal inlets because the variation in cross-sectional area is likely due to several factors in addition to the total discharge.

SCALING TIDAL INLETS IN MOVABLE-BED MODELS

Movable-bed physical models of jettied and unjettied inlet systems have seen limited use (JAIN and KENNEDY, 1979) due to uncertainty about similitude relationships for scaling model results to the scale of full-size inlets (prototype scale). One confounding result has been the failure of model results to conform to the established equilibrium area versus tidal prism relations as shown on Figure 1, giving rise to speculation about adverse scaling effects. Consequently, most movable-bed inlet model results were viewed as qualitative indicators of general inlet behavior and evolution, and little attempt has been made to use movable-bed models to quantify depth of scour or amount of deposition under given flow conditions.

Area constraints in laboratory facilities generally force the prototype-to-model geometric length scale (N_L) of a typical inlet to be on the order of 75-to-1 or greater ($N_L \geq 75$). For a model in which the flow kinematics conform to the Froude similitude relationship, it is not practical to reduce the model sediment size by the geometric length scale and still have noncohesive sediment in the model. Instead, noncohesive sediment is used in the model that has a grain-size diameter relatively larger than the diameter required by Froude scaling. The consequence is that model currents need to be relatively faster than currents specified by Froude scaling to move the sediment and scour the inlet channel to a depth similar to what would occur in nature. Therefore, it is necessary to *"distort"* the prototype-to-model velocity scale to achieve similarity in scour patterns between model and prototype-scale inlets. Unfortunately, distorting the velocity scale limits the movable-bed inlet model to situations where inlet channel scour is caused solely by currents without any wave action.

The tidal prism versus minimum inlet cross-sectional area relationship derived in this paper appears to apply to both full-scale and model-scale inlets equally well as shown in Figure 8. This implies that any movable-bed scaling law should maintain this "tidal prism relationship" between model and prototype.

In the following section a movable-bed modeling relationship is derived that is suitable for movable-bed modeling of inlet channel scour problems stemming from bedload sediment transport caused by tidal currents. Such scour is most common in the throat of inlet systems where waves have only a secondary effect because of reduced wave height or fairly deep channel depths. Situations where waves are thought to be a contributing scour mechanism are **NOT** correctly simulated by the relationship derived below.

Scaling Relationship Derivation

Appropriate similitude relationships can be established by assuring that dominant physical features and responses in the physical model are similar to the prototype that it represents (HUGHES, 1993). For tidal inlet throat sections it is important that the tidal prism relationship of Eqn. 42 is the same in the model as in the prototype.

First, Eqn. 42 is arranged into the form of a dimensionless parameter, *i.e.*,

$$\mathcal{F} = \frac{0.87}{A_c}\left[\frac{W^{1/9}}{|g(S_s - 1)|^{4/9}d_c^{1/3}T^{8/9}}\right]P^{8/9} \qquad (45)$$

Similarity requires that the value of dimensionless number $\mathcal{F}$ be the same in model as in prototype. Equating $\mathcal{F}_{\text{prototype}} = \mathcal{F}_{\text{model}}$, rearranging into a form containing prototype-to-model ratios of each variable, and representing each of the parameter ratios as an uppercase N with the variable listed as the subscript results in

$$\frac{N_W^{1/9}N_P^{8/9}}{N_{A_c}N_{|S_s-1|}^{4/9}N_{d_c}^{1/3}N_T^{8/9}} = 1 \qquad (46)$$

where, for example, the scale ratio $N_W = W_{\text{prototype}}/W_{\text{model}}$. The gravity scale N_g is equal to unity and has been omitted.

Because the tidal inlet model is a *long wave model* where vertical velocities and accelerations are expected to be small compared to horizontal components, there is a possibility of having a geometrically distorted model where the horizontal and vertical length scales are different. The possibility of a geometrically distorted model is retained by defining the horizontal length scale as N_X and the vertical length scale as N_Z. Thus, the following scale ratios can be expressed in terms of length scales: $N_W = N_X$; $N_{A_c} = N_X \cdot N_Z$; and $N_P = N_X^2 \cdot N_Z$. Making these substitutions into Eqn. 46 and solving for the time scale yields

$$N_T = \frac{N_X}{N_Z^{1/8}N_{|S_s-1|}^{1/2}N_{d_c}^{3/8}} \qquad (47)$$

where

N_T—tidal period scale $|=T_p/T_m|$

N_X—horizontal length scale $|=X_p/X_m|$

N_Z—vertical length scale $|=Z_p/Z_m|$

$N_{|S_s-1|}$—sediment immersed specific gravity scale

$\qquad |=(S_s - 1)_p/(S_s - 1)_m|$

N_{d_c}—sand grain size scale $|=(d_c)_p/(d_c)_m|$

and the subscripts p and m represent *prototype* and *model*, respectively. For a geometrically undistorted model where N_X and N_Z both equal the same length scale, N_L, Eqn. 47 reduces to

$$N_T = \frac{N_L^{7/8}}{N_{|S_s-1|}^{1/2}N_{d_c}^{3/8}} \qquad (48)$$

Furthermore, if it were possible to reduce the grain size according to the length scale, N_L, and the sediment relative density was the same as the prototype, the Froude time scale would be recovered.

In the same manner as above the distorted velocity scale

is found by expressing Eqn. 41 as a dimensionless number, i.e.,

$$\mathcal{G} = \frac{3.69}{Q_m}\left[\frac{|g(S_s - 1)|^{1/2}d_c^{3/8}}{W^{1/8}}\right]A_c^{9/8} \qquad (49)$$

then requiring $\mathcal{G}_{\text{prototype}} = \mathcal{G}_{\text{model}}$, and finally expressing the result in terms of scale ratios. Noting as before, $N_W = N_X$; $N_{A_c} = N_X \cdot N_Z$ and by definition, $N_{Q_m} = N_V \cdot N_{A_c}$, which when substituted yields the "distorted" velocity scale

$$N_V = N_{|S_s - 1|}^{1/2}N_{d_c}^{3/8}N_Z^{1/8} \qquad (50)$$

The velocity scale depends on the vertical length scale, but not the horizontal length scale. For geometrically undistorted models replace N_Z with N_L. Once again, the Froude velocity scale is recovered for the improbable special case of $N_{d_c} = N_L$ with model relative density the same as the prototype.

Combining Eqns. 47 and 50 results in the obvious identity $N_V = N_X/N_T$. Finally, note that the same velocity scaling relationship given by Eqn. 50 will be produced when the expression for equilibrium scour depth mean velocity (Eqn. 12) is preserved between model and prototype. This means that the small-scale model maintains the same relative shear stress balance between the flow and sediment as occurs in the prototype regime. Also implied is the existence of fully-rough turbulent flow in the model so that critical shear stress can be represented by Eqn. 6.

YALIN (1971) noted that fully-rough conditions existed when the grain-size Reynolds number exceeded 70, i.e.,

$$\mathbf{R}_c = \frac{v_* k_s}{\nu} > 70 \qquad (51)$$

where v_* is friction velocity ($= \sqrt{\tau_o/\rho_w}$), τ_o is bottom shear stress, ρ_w is water density, k_s is roughness, and ν is kinematic viscosity of the fluid. Determining whether fully-rough flow exists in small-scale physical models is difficult due to uncertainty in specifying a value for roughness, k_s. For example, values of $\mathbf{R}_c$ in MAYOR-MORA'S (1977) experiments would exceed 70 at critical shear stress if the roughness was specified at a value greater than 3 mm (about 9 times the grain diameter). From the size of the ripples developed in the movable-bed model, a roughness of $k_s = 3$ mm is probably conservative, and it is reasonable to assume that fully-rough flow existed. However, designers of small-scale movable-bed models using the proposed guidance should evaluate the flow conditions to assure compliance with the fully-rough flow criterion.

Scaling Relationship Discussion

The $N_{|S_s - 1|}$ scale ratio allows use of model sediment having different density than the prototype. However, for practical reasons quartz sand is typically used in models so normally $N_{|S_s - 1|} \approx 1$. The N_{d_c} scale ratio in Eqn. 50 compensates for model sediment that is relatively larger than if it had been geometrically scaled according to the length scale, N_L, as required by strict geometric scaling. Consequently, the velocity scale in Eqns. 50 is a *distorted* velocity scale. In other words, the sediment grains in the model are larger than they should be, so the model currents need to be faster than Froude-

scaled currents in order to achieve the same equilibrium depth of scour.

The scaling relationships derived in this paper reduce sediment scale effects by attempting to assure that the balance between the boundary layer shear stress acting on the bottom and the critical shear stress of the bed material is preserved in the model. This *"shear stress balance"* restricts the modeling technology to portions of real inlets with the following characteristics:

- Bottom scour is primarily due to the tidal current
- Concurrent wave action is small and does not contribute significantly to sediment transport
- Sediment is transported in bedload mode (approaching equilibrium)
- Sediment is noncohesive with only minor cohesive components

Typical inlet regions and processes that could be modeled using this proposed scaling guidance include the following:

(1) All or portions of a structured or unstructured inlet throat section can be modeled. (However, attempting to model entire throat sections for large inlets may not be practical without introducing geometric distortion.)
(2) Jet flow features created by inlet jetty planform geometry will be reproduced by the model, and the model bed evolution will respond accordingly. (However, the relatively faster model velocity of the jet will enhance flow entrainment at the jet boundary, and this effect needs to be analyzed.)
(3) Localized bed evolution adjacent to the channel side of jetty structures will be correctly simulated, as will scour at the tip of training structures. Scour at free-standing bridge piers will probably not be in similitude because the dominant *"horseshoe vortex"* causing scour at vertical piers and piles is a different mechanism than the shear-stress balance assumed in this scaling relationship derivation.
(4) Changes in channel depth brought about by jetty modification and extension, construction of additional structures, and navigation channel realignment can be simulated. However, regions of deposition will require a source of infilling sediment.

Three caveats apply to movable-bed modeling of the situations described above. First, this modeling technology pertains only to the equilibrium condition where the movable bed no longer evolves. *Sediment transport rates* and the *time required to reach equilibrium* are **NOT** correctly simulated in the movable-bed model. In other words, the model will provide reasonable predictions of the final equilibrium bed configuration, but no information is gained regarding how long this evolution will take in the real world. This is actually beneficial because it precludes having to simulate tidal cycles in the model. At real inlets, the final equilibrium condition is maintained for the most part by currents at or around the peak ebb or flood flow. During the rest of the tide stage, currents are reduced and sediment motion is greatly reduced. Therefore, in the movable-bed model we only need to simu-

Table 2. *Movable-bed model parameters.*

Parameter	Prototype	Model
Width (W)	250 m	3.3 m
Maximum Depth (h_o)	15 m	0.2 m
Sediment (d_e)	0.4 mm	0.13 mm
Maximum Velocity (V_{max})	1.5 m/s	0.57 m/s
Maximum Discharge (Q_m)	3,000 m³s	0.2 m³/s
Tidal Period (T)	44,713 s	1,558 s

late the maximum flow condition long enough to achieve an equilibrium.

The second caution applies to deposition areas in the movable-bed model. Sediment deposition will occur in areas where the local flow velocity falls below the sediment incipient motion threshold. Sediment moved into this region is deposited. The scaling premise of the movable-bed model scaling relationship covers this situation, but there must be available sediment in order to have deposition. At real inlets, sediment sometimes comes from regions of the inlet that are actively scouring because of structural modification or change in flow condition. However, most sediment moving through an inlet is being continually introduced via the longshore drift. Therefore, if a sediment deposition problem such as channel infilling is to be studied in a movable-bed model, it is necessary to introduce the correct quantity of sediment into the model at the appropriate locations.

Finally, care must be taken for geometrically distorted models because slopes in the distorted models need to be relatively steeper than the prototype. However, the channel side slopes in the model can not be steeper than allowed by the natural angle of repose of the sediment; and consequently, maximum allowable slope conditions in the prototype will not be reproduced. Geometric distortion also introduces questions about correct reproduction of turbulent flow in regions of flow separation and entrainment, and further study is needed to answer these questions. In the interim, models should be geometrically undistorted if flow separation plays an important role in the inlet to be modeled.

As a modeling example, consider an inlet with the parameters given in the "Prototype" column of Table 2. Simulating this inlet in a movable-bed model with 0.13 mm quartz sediment gives a sediment grain-size scale of N_{d_e} = 3.08. For a length scale of N_L = 75 Eqn. 50 gives a velocity scale of N_V = 2.6, and a discharge scale of $N_Q = N_V \cdot N_L^2$ = 14,680. The time scale for the tidal period is found from Eqn. 48 as N_T = 28.7. If instead, Froude scaling were used, the velocity scale would be $N_{V_{Froude}}$ = 8.7, and the model velocity would need to be about 0.17 m/s which is beneath the incipient motion threshold for the model sediment.

SUMMARY AND CONCLUSIONS

A relationship is derived between the tidal prism, P, passing through an inlet during half of the spring tide cycle and the inlet throat minimum cross-sectional area, A_c. The relationship closely resembles the established empirical relationships of O'BRIEN (1931, 1969) and JARRETT (1976). The main assumption in the derivation is that the maximum discharge

per unit width through an inlet is at equilibrium with every depth across the minimum cross section. In other words, an increase in discharge would cause additional scour to occur; therefore, the predicted cross-sectional area is the absolute minimum for that flow condition.

The scaling coefficient in the derived tidal prism relationship is strongly influenced by tidal period, with sediment mean grain size and inlet width having only minor influence. This same correspondence appears in the scaling coefficient derived by KRAUS (1998), who also included the effect of alongshore sediment transport.

The derived minimum A_c versus P relationship shows good correspondence to data from 102 tidal inlets from around the United States coastline with most inlets having an equilibrium area larger than the minimum predicted. More importantly, because of the inclusion of tidal period, the relationship also shows good correspondence to equilibrium results obtained from 18 small-scale movable-bed laboratory experiments. Previous empirical relationships with constant scaling coefficients had under predicted small-scale model cross-sectional areas by an order of magnitude.

As noted, most of the inlet equilibrium cross-sectional areas are larger than the minimums predicted by the derived relationship. This is caused by a number of factors that vary between inlets. Some inlets may have different primary flow channels during ebb and flood tide which could be caused by jetty structures directing the flow patterns or perhaps by channel dredging activities. In these cases there are portions of the cross-section that carry less than the maximum discharge during each stage of the tide resulting in an equilibrium area greater than the minimum predicted. Likewise, inlet meandering at unstructured inlets results in multiple channels with some channels in equilibrium with the flow and older channels carrying less flow than in the past. Finally, variations in longshore sediment transport and the flow efficiency of the inlet throat in moving sediment through the inlet will contribute to differences in cross-sectional area as represented by the processes-based model developed by KRAUS (1998).

A constant empirical coefficient was added to the derived tidal prism relationship to provide a best fit to the full-scale and small scale inlet observations. The resulting equations provide reasonable estimates, but they do not show any real improvement over Jarrett's empirical expressions. In fact, JARRETT (1976) provided specific empirical relationships for different coasts and structural improvements, so his empirical results should provide better estimates for real inlets. The possible causes listed above for inlet area variations about the average are highly specific to each inlet, so any improvement to a theoretical tidal prism relationship will require inclusion of more physical processes to better represent the diverse peculiarities of the various types of inlets.

The data show conclusively that the "mean maximum velocity" ($V_{MAX} = Q_m/A_c$) is not too useful of a parameter for characterizing tidal inlets. The wide variation in values of V_{MAX} stem directly from the significant variation of equilibrium areas relative to the theoretical minimum cross-sectional area.

Finally, the fact that the derived tidal prism relation

worked equally well for small-scale laboratory inlets led to new scaling relationships for movable-bed modeling of tidal inlet throat regions where waves have minor influence. The derived time and velocity scales are different than conventional Froude scaling in order to compensate for using larger sediment grain sizes in the model than dictated by strict geometry similitude. The same distorted velocity scale arises from assuring the expression for equilibrium maximum discharge per unit width is similar between the model and prototype. This means that the relative balance between the turbulent shear stress acting on the bottom and the critical shear stress of the bed material must be the same in the model as in prototype.

The movable-bed scaling relationships are perhaps the most important result given in this paper because the scaling will allow quantitative results of complicated inlet processes to be obtained from properly operated small-scale movable-bed inlet models.

ACKNOWLEDGEMENTS

LITERATURE CITED

BRUUN, P., 1978. *Stability of Tidal Inlets—Theory and Engineering.* Amsterdam: Elsevier Scientific Publishing, Developments in Geotechnical Engineering, Vol 23.

BYRNE, R. J.; GAMMISCH, R. A., and THOMAS, G. R., 1980. Tidal Prism-Inlet Area Relations for Small Tidal Inlets. *Proceedings of the 17th International Coastal Engineering Conference* (American Society of Civil Engineers, New York) Vol 3, pp. 2517–2533.

CARR, E. E., 1999. An Examination of Flood Deltas at Florida's Tidal Inlets. *Technical Report UFL/COEL-99/015,* Coastal and Oceanographic Engineering Laboratory, University of Florida, Gainesville, Florida.

HUGHES, S. A., 1993. *Physical Models and Laboratory Techniques in Coastal Engineering.* Singapore: World Scientific Publishing, Advanced Series on Ocean Engineering—Volume 7.

HUGHES, S. A., 2000. Effect of Offset Jetties on Tidal Inlet Flood Flow. *Shore and Beach,* 68 (1), 31–38.

JAIN, S. C. and KENNEDY, J. F., 1979. An Evaluation of Movable-Bed Tidal Inlet Models. *GITI Report 17,* US Army Engineer Waterways Experiment Station, Vicksburg, Mississippi.

JARRETT, J. T., 1976. Tidal Prism—Inlet Area Relationships. *GITI Report 3,* US Army Engineer Waterways Experiment Station, Vicksburg, Mississippi.

JOHNSON, J. W., 1972. Tidal Inlets on the California, Oregon, and Washington Coasts. *Technical Report HEL 24-12,* Hydraulic Engineering Laboratory, University of California at Berkeley, Berkeley, California.

KEULEGAN, G. H. and HALL, J. V., Jr., 1950. A Formula for the Calculation of the Tidal Discharge Through an Inlet. *Bulletin of the Beach Erosion Board,* 4 (1), 15–29.

KRAUS, N. C., 1998. Inlet Cross-Section Area Calculated by Process-Based Model. *Proceedings of the 26th International Coastal Engineering Conference* (American Society of Civil Engineers, New York), Vol 3, pp. 3265–3278.

KRISHNAMURTHY, M., 1977. Tidal Prism of Equilibrium Inlets. *Journal of the Waterway, Port, Coastal and Ocean Division* (American Society of Civil Engineers, New York), 103(WW4), 423–432.

LACEY, G., 1929. Stable Channels in Alluvium. *Proceedings, Institute of Civil Engineers,* 229, 250–285.

LECONTE, L. J., 1905. Discussion of Notes on the Improvement of River and Harbor Outlets in the United States. Paper No. 1009 by D. A. Watts, *Transactions, American Society of Civil Engineers,* LV, 306–308.

MASON, C., 1973. Regime Equations and Tidal Inlets. *Journal of the Waterways, Harbors and Coastal Engineering Division.* (American Society of Civil Engineers, New York), 99(WW3), 393–397.

MAYOR-MORA, R. E., 1977. Laboratory Investigation of Tidal Inlets on Sandy Coasts. *GITI Report 11,* US Army Engineer Waterways Experiment Station, Vicksburg, Mississippi.

NAYAK, I. V., 1971. Tidal Prism-Area Relationship in a Model Inlet. *Technical Report HEL 24-1,* Hydraulic Engineering Laboratory, University of California at Berkeley, Berkeley, California.

O'BRIEN, M. P., 1931. Estuary Tidal Prisms Related to Entrance Areas. *Civil Engineering,* 1(8), 738–739.

O'BRIEN, M. P., 1969. Equilibrium Flow Areas of Inlets on Sandy Coasts. *Journal of the Waterways and Harbors Division* (American Society of Civil Engineers), 95(WW1), 43–52.

O'BRIEN, M. P., 1976. Notes on Tidal Inlets on Sandy Shores. *GITI Report 5,* US Army Engineer Waterways Experiment Station, Vicksburg, Mississippi.

SEABERGH, W. C.; KING, D. B., and STEPHENS, B. E. 2001. Tidal Inlet Equilibrium Area Experiments, Inlet Laboratory Investigations, ERDC/CHL TR-01-02, U.S. Army Engineer Research and Development Center, Vicksburg, Mississippi.

SIMONS, D. B. and ALBERTSON, M. L., 1963. Uniform Water Conveyance Channels in Alluvial Materials. *Transactions, American Society of Civil Engineers,* 128(I), 65–107.

THOMAS, W. A. and PRASUHN, A. L., 1977. Mathematical Modeling of Scour and Deposition, *Journal of the Hydraulics Division,* American Society of Civil Engineers, 103(HY8), 851–863.

YALIN, M. S., 1971. *Theory of Hydraulic Models.* London: MacMillan.

SYMBOLS

A_e — minimum equilibrium cross-sectional area
a_t — tidal amplitude
C — dimensional coefficient in the A_e versus P relationship
C_e — constant of proportionality
C_I — tidal prism factor
C_k — non-sinusoidal tide factor ($0.81 \leq C_k \leq 1.0$)
C_s — constant of proportionality
C_τ — undetermined constant
d_e — median grain-size diameter
f_s — sediment function
g — gravitational acceleration
h — water depth
h_e — equilibrium water depth at maximum discharge
h_o — maximum cross-section water depth
k — exponent in the A_e versus P relationship
k_a — empirical constant
k_s — roughness of bed material

m – subscript representing *model*

n – Manning coefficient in units of s/m$^{1/3}$

N – prototype-to-model scale ratio

N_{d_c} – sand grain size scale $[= (d_c)_p/(d_c)_m]$

N_L – undistorted length scale $[= L_p/L_m]$

N_Q – discharge scale $[= Q_p/Q_m]$

$N_{|S_S-1|}$ – sediment immersed specific gravity scale $[= (S_S - 1)_p/(S_S - 1)_m]$

N_T – tidal period scale $[= T_p/T_m]$

N_V – horizontal velocity scale $[= V_p/V_m]$

N_X – horizontal length scale $[= X_p/X_m]$

N_Z – vertical length scale $[= Z_p/Z_m]$

p – subscript representing *prototype*

P – tidal prism

Q – time-varying total discharge

q_c – equilibrium discharge per unit width

Q_g – gross longshore sediment transport rate

Q_m – total maximum discharge

R – inlet hydraulic radius at minimum cross section

R_e – grain size Reynolds number

S – channel slope in Manning's Equation

S_b – bay surface area

S_S – sediment specific gravity $[= \rho_s/\rho_w]$

t – time

T – tidal period

V – velocity in the water column

V_m – depth-averaged velocity

V_{max} – maximum velocity of the vertical velocity profile

V_{MAX} – mean velocity at maximum discharge averaged over inlet throat $[= Q_m/A_c]$

v_* – friction velocity $[= \tau_o/\rho_w]$

W – equilibrium channel width at minimum cross section

y – cross channel length dimension

Greek Symbols

α – empirical coefficient ≈ 1.0

Γ – mathematical Gamma function

η – time-dependent tide elevation

ν – kinematic viscosity of fluid

π – mathematical Pi

ρ_s – mass density of sand

ρ_w – mass density of water

τ_{cr} – critical shear stress of noncohesive sand

τ_o – shear stress at the bed from fully developed flow

Ψ – Einstein's flow intensity parameter

Other Symbols

$\mathcal{F}$ – dimensionless parameter

$\mathcal{G}$ – dimensionless parameter